BNL-62698

JOURNAL OF GEOPHYSICAL RESEARCH, VOL. 101, NO. D22, PAGES 29,123–29,135, DECEMBER 20, 1996

Physical and chemical observations in marine stratus during the 1993 North Atlantic Regional Experiment: Factors controlling cloud droplet number concentrations

W.R. Leaitch, C.M. Banic, G.A. Isaac, M.D. Couture, P.S.K. Liu, I. Gultepe and S.-M. Li

Atmospheric Environment Service, Downsview, Ontario, Canada

L. Kleinman and P.H. Daum

Brookhaven National Laboratory, Upton, New York

J.I. MacPherson

National Research Council of Canada, Ottawa, Ontario

Abstract. Airborne observations from 14 flights in marine stratus over the Gulf of Maine and Bay of Fundy in August and September of 1993 are examined for the relationships among the cloud droplet number concentrations (N_d), the out-of-cloud aerosol particle number concentrations (N_a), the major ion concentrations in the cloud water, and turbulence in cloud. There was a wide range of aerosol concentrations, but when low stratus and the main anthropogenic plume from eastern North America were in the same area the plume overrode the cloud. The N_d increased with increasing N_a and cloud water sulfate concentration ($cwSO_4^=$), but the relationships were very weak. The separation of the data between smooth and lightly turbulent air substantially improved the ability to explain the variance in the N_d by either of these two quantities. Also, the relative increase in N_d for increases in N_a and $cwSO_4^=$ was greater for lightly turbulent air than for smooth air. The estimated minimum size of particles activated in these clouds ranged from 0.14 μm to 0.31 μm, corresponding to average supersaturations of $<0.1\%$. The minimum size tended to be lower for lightly turbulent air and smaller N_a. The results for lightly turbulent air agree well with previously reported parameterizations of the impact of aerosols on N_d, but the results for smooth air do not agree. In general, more knowledge of the physical factors controlling the N_d in stratiform clouds, such as turbulence, is needed to improve not only our ability to represent N_d but also to increase our understanding of the impact of the aerosol particles on the N_d and climate.

1. Introduction

Changes in aerosol properties can alter the microphysical properties of clouds, which alters the shortwave reflectance properties of the clouds. This process, known as the indirect aerosol effect [*Charlson et al.*, 1992], is an important concern for climate change. For example, *Jones et al.* [1994] reported estimates for the indirect aerosol effect of -1.3 W m^{-2} based on the results from a general circulation model. Still, there continues to be a great deal of uncertainty in our understanding of this effect [*Penner et al.*, 1994; *Intergovernmental Panel on Climate Change (IPCC)*, 1994].

A number of studies have demonstrated links between cloud droplet number concentrations (N_d) and certain aerosol quantities [more recently, *Leaitch et al.*, 1992; *Raga and Jonas*, 1993; *Martin et al.*, 1994; *Gillani et al.*, 1995]. However, *Novakov et al.* [1994] found no observable trend between N_d and non-sea-salt sulfate concentrations for cumulus and a weak relationship for stratocumulus. They argued that mixing processes in their clouds obscured the tendencies. *Anderson et al.* [1994] were unable to detect an unambiguous link between the N_d and the aerosol, due to a combination of mesoscale and turbulent factors, noting that turbulence measurements were essential to quantifying the aerosol influence on cloud microphysics. *Arends et al.* [1994] also referred to the importance of turbulence in determining the microphysical characteristics of clouds. Turbulence may be important to the determination of the N_d for reasons other than its influence on mixing processes; it affects the ascent rate of air parcels in cloud, which determines the cooling rate and hence may influence the maximum cloud supersaturation.

It is critical to understand the indirect aerosol effect for marine stratus. Since these clouds have large spatial extent, are relatively thin, and cover a low-albedo surface, the planetary

Copyright 1996 by the American Geophysical Union.

Paper number 96JD01228.
0148-0227/96/96JD-01228$09.00

albedo is more sensitive to aerosol-induced changes in their microphysics compared with other clouds [e.g., *Penner et al.*, 1994]. The 1993 intensive of the North Atlantic Regional Experiment (NARE) offered the opportunity to conduct airborne measurements in marine stratus which frequently form over the cool waters of the Gulf of Maine and Bay of Fundy in the summer. This region is impacted by air masses with widely varying aerosol and trace gas loadings [*Banic et al.*, this issue; *Kleinman et al.*, this issue (a, b)]. The observations made near and in these low clouds are used to address the indirect aerosol effect in this region for the smooth-air and light- turbulence conditions seen. The influence of the out-of-cloud concentrations of accumulation-mode aerosol particle (N_a) on the N_d is studied; the minimum sizes of particles activated in these clouds are estimated; and the concentrations of the major ions in the cloud water are related to the N_a and N_d. Comparisons are drawn with previous work. Cloud parameterizations for use in general circulation models, based on the same data set, have been developed by *Gultepe et al.*, [1996].

2. Experiment

The operations were based at Yarmouth, Nova Scotia, at the southern end of the Nova Scotia peninsula (Figure 1). The sampling platform was the National Research Council of Canada DHC-6 Twin Otter aircraft, with an operating airspeed of 50-70 m s^{-1}. Fourteen flights were conducted in and around low-level stratus (i.e. < 850 m-MSL) over the Gulf of Maine and Bay of Fundy on 10 days between August 13 and September 8, 1993. All sampling was within 50 km of Yarmouth, usually to the south, with the exception of one flight from Saint John, New Brunswick.

Several quantities pertaining to the chemistry, microphysics and dynamics of the clouds were measured, as well as aerosol particle microphysics. The instrumentation on the Twin Otter pertinent to the present study is described below. Complementing this study is a detailed characterization of the aerosols at Chebogue Point [*Liu et al.*, this issue], the NARE intensive surface site 10 km south of Yarmouth.

The size distributions of aerosol and cloud particles were determined using two Particle Measuring Systems (PMS) probes mounted under the wings of the aircraft. Each probe uses the scattering of laser light to detect and size particles. Aerosol particles from 0.13 to 3 μm diameter were measured with a passive scattering aerosol spectrometer probe (PCASP)-100X which sizes particles into one of fifteen size bins. The PCASP-100X includes a diffuser nozzle to decelerate the particles before sampling. Deicing heaters in this section ensured that the out-of-cloud aerosol was dried before detection. For long times in cloud, as when sampling stratus, and when larger droplets are present (i.e., > 12 μm), it appears that the interior of the probe diffuser is wetted by the continuous accumulation of cloud droplets. Under these conditions the probe can completely dry relatively few of the cloud droplets. However, the data indicate that the cloud interstitial particles were dried during sampling. The sizing calibrations, given in Table 1, were performed with nearly monodisperse N_aCl and latex particles following *Liu et al.* [1993]. The sampling of sulfate particles with this probe may be subject to some uncertainty, due to the response of the probe to particles of different indices of refraction, as *Kim* [1995] has shown for the sampling of 0.4 to 0.8 μm particles with a PMS-ASASP. Particles and cloud droplets from 2 to 35 μm were sampled non-intrusively with a forward scattering spectrometer probe (FSSP-100). Calibrations were done with nearly monodisperse latex particles and glass beads, and the N_d have been corrected for dead time and coincidence following *Baumgardner et al.* [1985]. Larger cloud and precipitation-size particles were sampled with a PMS 2D grey-scale probe. This is also a nonintrusive probe which uses the shadowing of a laser beam against an array of diodes to count and size, in two dimensions, particles >25 μm passing through the detection area. Calibrations of this probe were performed with glass beads.

The cloud liquid water content (LWC) measurement was made with a wing-mounted PMS King heated-wire probe. The uncertainty in the LWC using the King probe is estimated at $\pm(0.1 \times LWC + 0.02)$ g m^{-3} [*Cober et al.*, 1995].

Cloud water was collected using modified slotted-rod collectors as described by *Leaitch et al.* [1992]. The collectors were deployed out of the top of the fuselage ahead of the propellers. Samples were analyzed for a variety of species: major inorganic and organic ions, H_2O_2, trace metals, dissolved HCHO and black carbon. The present discussion considers only the inorganic and organic ions. The black carbon results are given by *Chylek et al.* [this issue], and the other measurements have not been reported. The major ions were analyzed by ion chromatography as described by *Li et al.* [this issue]. Samples used for acetate and formate were frozen within 2 hours of collection and kept frozen until analyzed.

A noseboom-mounted Rosemount 858 five-hole probe and a Litton 90-100 Inertial Reference System were used to measure the three orthogonal components of atmospheric motion and the resultant wind speed and direction over a frequency range of 0-5 Hz [*MacPherson*, 1990; *Angevine and MacPherson*, 1995]. Only the vertical gust measurements (w') are used here. The standard deviation of w' ($\sigma_{w'}$) is used as a measure of turbulence in the clouds. The uncertainty in $\sigma_{w'}$, estimated from intercomparisons with other aircraft, is ± 0.05 m s^{-1}.

All real-time data were sampled at > 1 Hz, and the subsequent analyses are based on 1-s-averaged data points.

3. Observations

3.1. Source Regions and Boundary Layer Structure

Figure 1 shows the air back trajectories at 1000 mbar and 925 mbar, determined with the three-dimensional method of *Olson et al.* [1978], for the 14 flights discussed here. Following the arguments of *Brook et al.* [1993], the uncertainty in these trajectories at three days back is estimated at $\pm$400 km. The 1000 mbar trajectories show that the air arrived from the north, east, and south. At 925 mbar the air flow was mostly from the west off the continent. In five cases (flights 8, 14, 16, 21, 36), the 925 mbar and 1000 mbar trajectories were of similar origin. The cloud measurements were made at pressures ranging from 920 mbar to 1005 mbar (altitudes of 850 m to 100 m, respectively). The median pressure of the observations was 977 mbar, and 85% of the cases were sampled at > 950 mbar.

The clouds were formed as warmer air moved over the colder water off the south end of Nova Scotia and in the Bay of Fundy. The winds near the ocean were light during the study,

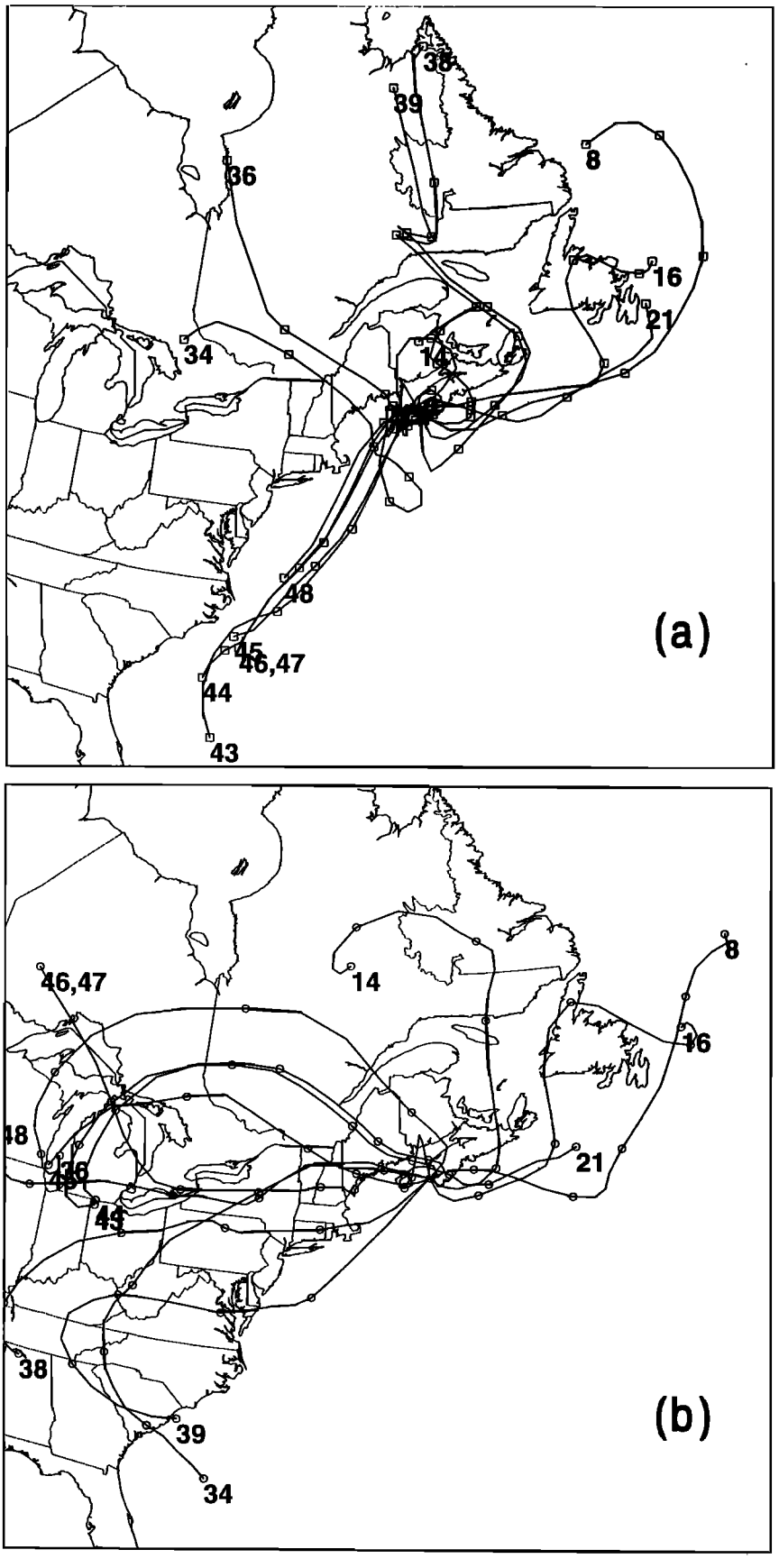

Figure 1. The (a) 1000 mbar and (b) 925 mbar air back trajectories ending at Yarmouth, Nova Scotia, calculated for the times of low-cloud flights using the method of *Olson et al.* [1978]. Increments are 1 day, and the flight number is given at the five-day back point.

Table 1. Sizing Calibration for this PCASP-100X

Channel	Diameter (μm)
1	0.125 - 0.135
2	0.135 - 0.16
3	0.16 - 0.18
4	0.18 - 0.205
5	0.205 - 0.26
6	0.26 - 0.31
7	0.31 - 0.40
8	0.4 - 0.5
9	0.5 - 0.7
10	0.7 - 0.9
11	0.9 - 1.2
12	1.2 - 1.5
13	1.5 - 2
14	2 - 2.5
15	2.5 - 3

resulting in generally calm seas. Sea surface temperatures and aspects of the boundary layer transport are discussed by *Angevine et al.* [this issue]. Light patchy drizzle was observed on five days, as indicated from the 2D grey-scale data. Figure 2 shows the N_a (from the PCASP), N_d (from the FSSP), LWC, temperature, and theta Q (potential temperature conservative for condensation and precipitation processes) from four profiles through cloud over the ocean. These profiles illustrate some of the variability seen during the study. The cloud thicknesses ranged from about 50 m to 250 m in the cases shown in Figure 2 and were <300 m for all cases. In some cases, such as flight 43, thin layers were present. The profile data indicate that the aerosol concentration just below cloud is similar to the in-cloud N_a+N_d. The changes in the N_a above cloud are relatively small, except in the case of flight 45, where highly polluted continental air overrode the marine air. The LWC in three of the four cases increases steadily with height above the cloud base. The maximum LWC near the cloud tops

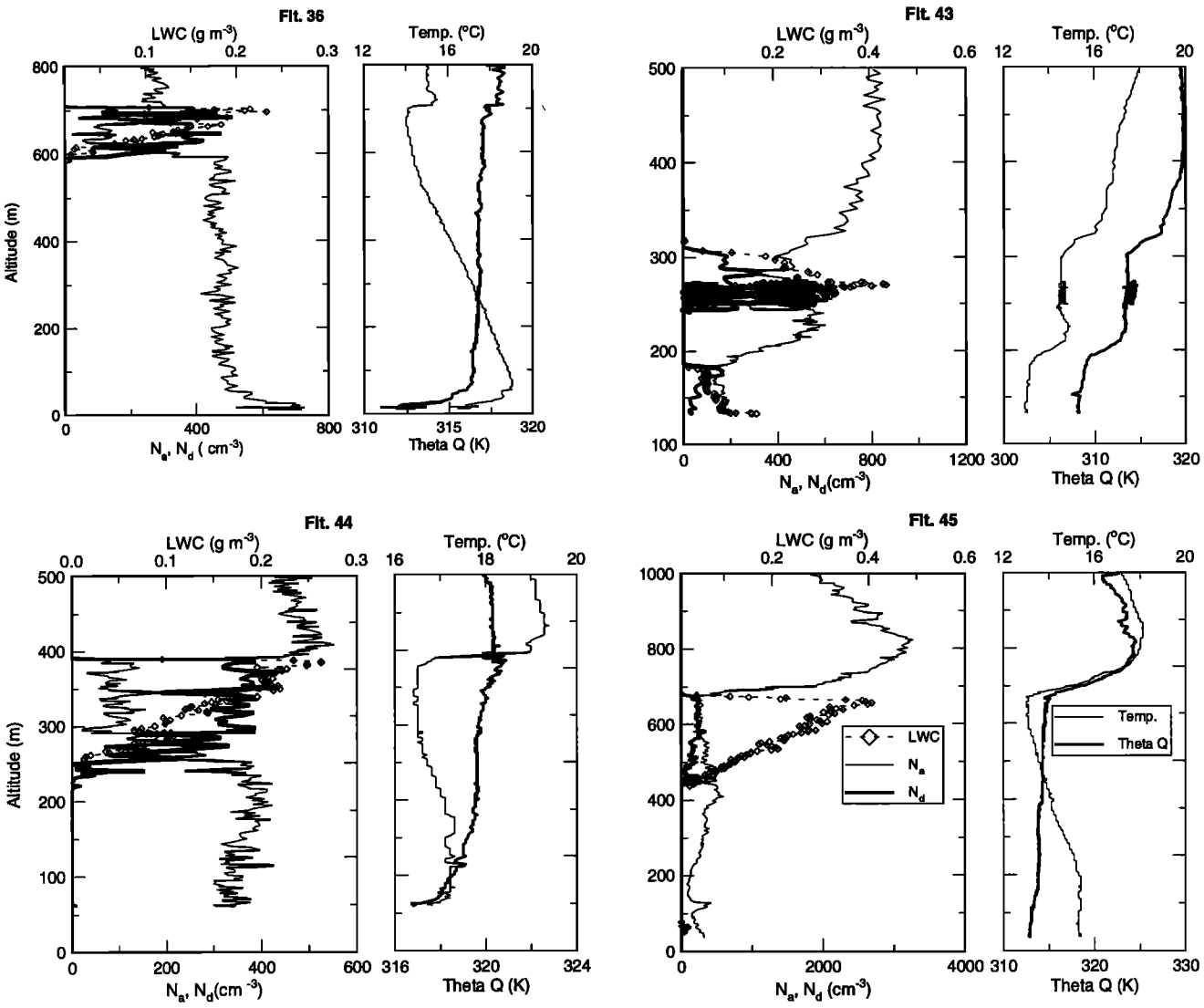

Figure 2. Vertical profiles of N_a, N_d, liquid water content (LWC), theta Q, and temperature for four flights with complete penetration of the low cloud.

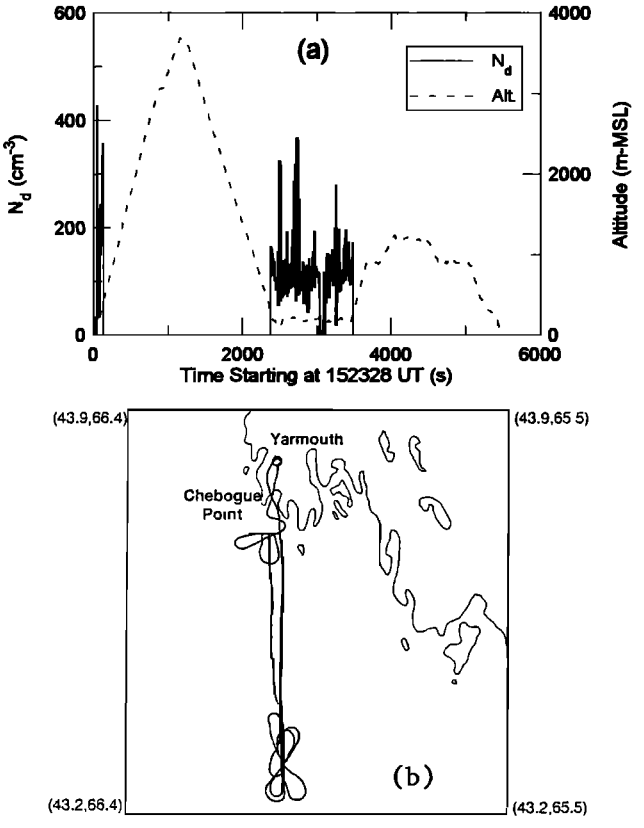

Figure 3. (a) Time series of N_d and altitude and (b) two-dimensional flight track of Twin Otter for flight 34.

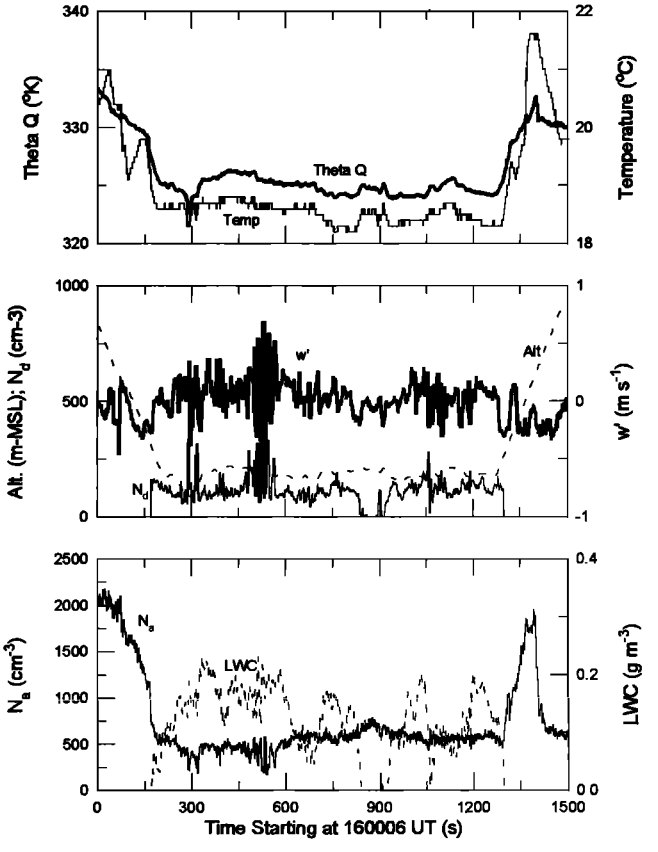

Figure 4. Time series of theta Q, temperature, w', N_d, altitude, N_a, and LWC for cloud-level segment of flight 34.

are about 80%, 50%, and 70% of the adiabatic value for flights 36, 44, and 45, respectively.

The air below the temperature inversions which cap the clouds exhibits varying characteristics. For flight 36 this air is mixed down to within 30 m of the ocean surface, where the temperature drops sharply. For flight 43, which took place across the Bay of Fundy, three nearly isothermal layers with different sources are indicated. Multiple layers are also seen for flights 44 and 45. The 1000 mbar and 925 mbar back trajectories for flights 43-45 have quite different histories. Flights 43, 44, and 45 have 1000 mbar trajectories coming from the south over the ocean, while the 925 mbar air came from the west off the continent. In contrast, the five-day histories for both the 1000 mbar and 925 mbar trajectories for flight 36 are continental and relatively close geographically. The one-day back trajectories are from along the Nova Scotia peninsula, which suggests the possibility that mixing over land from daytime heating was responsible for the greater depth of the mixed layer in this case.

The vertical wind gusts in these clouds were such that the air can be classified as smooth to lightly turbulent. The sources of the turbulence in these clouds have not been investigated but may be due to wind shear, cloud-top radiative cooling, latent heat release, mechanical stirring near the coastline, and for air coming off land over the cooler waters, incomplete decay of turbulence from surface heating over the land. Except in the case of the longwave motions (see below), the eddy sizes are estimated at 50-200 m.

3.2. Case Studies

Flights 34 and 14 from September 1 and August 17, respectively, are described here to illustrate some interesting features in the data, and to demonstrate the data processing applied to the complete cloud data set (14 flights). Figure 3a shows a times series of the aircraft altitude and the N_d for flight 34. The flight track is shown below in Figure 3b. The aircraft took off from Yarmouth at about 1524 UT, climbed through a thin cloud layer (capped at about 400 m MSL), and continued climbing to 3.8 km while heading to a location over the ocean about 50 km due south from Chebogue Point. The aircraft descended to about 100 m over the ocean, in cloud below about 300 m, and then flew north toward Chebogue Point in cloud at about 200 m. Approaching Chebogue Point, the aircraft climbed for a short sounding and then returned to Yarmouth.

Figure 4 shows the time series of the 1-s-averaged temperature, theta Q, Nd, w', altitude, N_a, and LWC for the period of cloud sampling during flight 34. The temperature in cloud was 18°-19 °C, and a sharp inversion capped the cloud. The aircraft was in continuous cloud at 200 m, except for a short period near 900 s. The variability in the w' is irregular and relatively small, except for intervals when there are distinctive oscillations (i.e., 250-400 s and 500-600 s). The $\sigma_{w'}$ for the air outside of these oscillations is 0.10 m s^{-1}, indicative of smooth air. The oscillations in w' at 500-600 s have a period of 10-20 s and indicate a wave motion. The N_d are relatively uniform at about

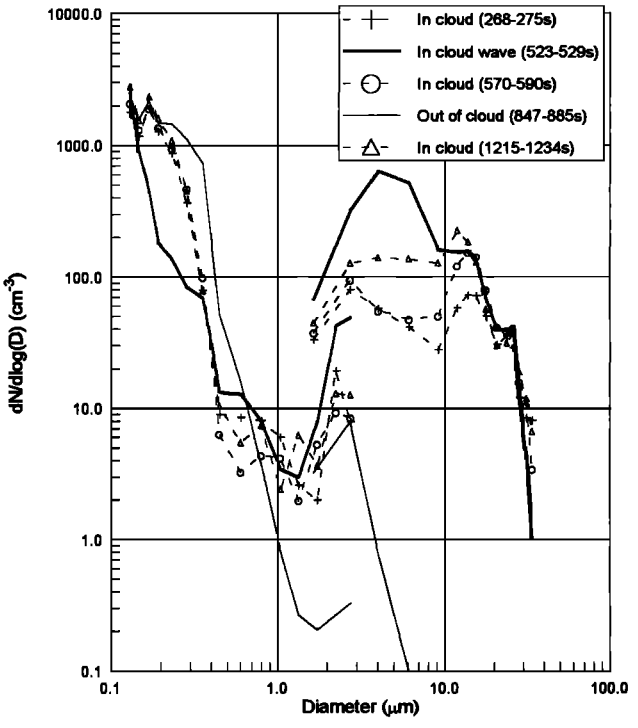

Figure 5. Aerosol particle and cloud droplet size distributions from the passive scattering aerosol spectrometer probe (PCASP) and forward scattering spectrometer probe (FSSP) for selected intervals in and out of cloud from flight 34.

100-150 cm^{-3}, except for the time out of cloud near 900 s and during the encounter with the wave when the N_d increase markedly. At 500-600 s the variations in N_d closely parallel the variations in the w'. The LWC shows some sensitivity to the wave motion at 500-600 s, but the relative changes in LWC are not nearly as large as those in the N_d. The N_a are relatively steady throughout the in-cloud period, except when affected by the wave which leads to decreases in the N_a coincident with increases in the N_d, indicating the additional scavenging of some of these particles. The increase in the N_d during the wave event relative to that in the smooth air (about 280 cm^{-3}) compares reasonably well with the decrease in the interstitial N_a for the wave event (about 360 cm^{-3}). This is a case of smooth air and relatively uniform cloud properties with an additional vertical forcing (wave) in a few areas. It is believed that localized increases in the cloud supersaturation resulted from the vertical motion of the wave, and this led to the activation of additional particles.

Size distributions of the interstitial aerosol particles and the cloud droplets (>2 μm) averaged over four in-cloud segments are shown in Figure 5. Three of the segments are for the smooth-air N_d (i.e., outside of the wave event: 268 to 275 s, 570 to 590 s, and 1215 to 1234 s) and one gives the spectrum corresponding to the maximum in the N_d coincident for the wave event at 523 to 529 s. Figure 5 also shows the aerosol spectrum averaged for the out-of-cloud period from 847 to 885 s. The interstitial spectra for the smooth-air N_d are close to the out-of-cloud aerosol spectrum from the smallest particles measured up to about channel 4 of the PCASP (about 0.21 μm) beyond which the interstitial spectra fall well below the out-of-cloud spectrum until particle sizes of about 0.5-0.7 μm. Partially dried droplets are evident in the levelling of the size distribution from about 0.5-2 μm. Thus the minimum size of particle activated, or the activation threshold, in this smooth-air case is about 0.21 μm. For the wave event, the interstitial spectrum is close to the out-of-cloud spectrum only for the first two channels of the PCASP and falls below the out-of-cloud spectrum for sizes larger than 0.16 μm. The increase in particle activation in the wave is matched by a reduction in the mean size of the cloud droplets relative to the smooth-air spectra. This is accomplished with a relatively small change in the LWC.

Cloud was sampled back and forth between Chebogue Point and the ocean end point (Figure 3b) on flight 14. Figure 6 shows the time series of temperature, theta Q, altitude, N_d, w', N_a, and LWC. Observations were made above and below the cloud before and after the in-cloud sampling. Temperature and theta Q are positively correlated, except near 1400 s, when the aircraft ascended slightly above the cloud during a turn. The small decrease in theta Q relative to the increase in temperature at the turn indicates drier air just above the cloud. After the turn, the aircraft retraced its path giving rise to the symmetry in the time series data about this time. The symmetry in the observations indicates that the aerosol and cloud properties were relatively constant over the sampling time (0.5 hours). There was some light turbulence inside cloud ($\sigma_{w'}$ is 0.19 m s^{-1}) compared with outside of cloud and compared with the smooth air inside cloud on flight 34. On average, the N_d are significantly higher in this case compared with flight 34, despite slightly lower N_a. The sum of the interstitial cloud N_a and the

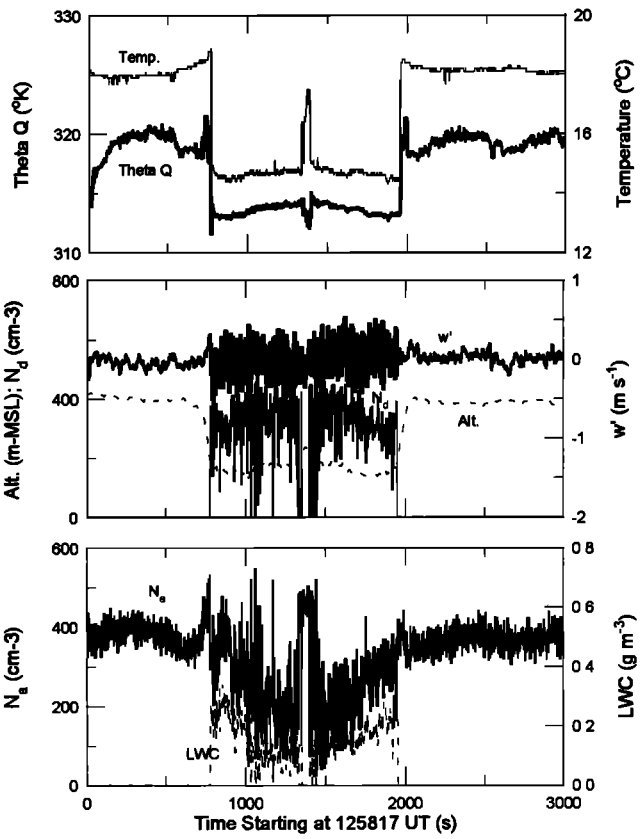

Figure 6. Time series of theta Q, temperature , w', N_d, altitude, N_a, and LWC for in-cloud segment of flight 14.

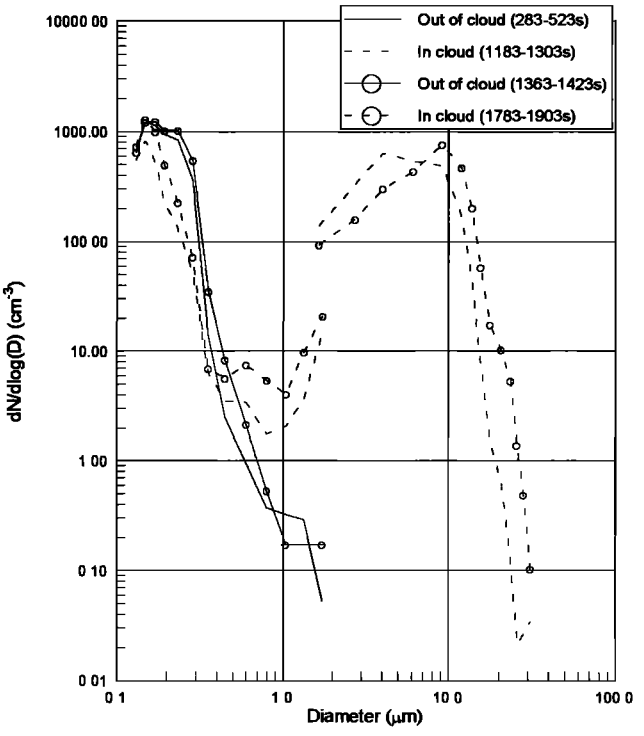

Figure 7. Aerosol particle and cloud droplet size distributions from the PCASP and FSSP for selected intervals in and out of cloud from flight 14

N_d is about 600 cm^{-3}, close to the Na maximum of about 550 cm^{-3}.

Two interstitial cloud particle spectra and two out-of-cloud particle spectra from flight 14 are shown in Figure 7. The interstitial spectra follow the corresponding out-of-cloud spectra from the smallest particles up to channels 2 to 3 of the PCASP and then fall below the out-of-cloud spectra until about 0.4 μm, after which evaporating droplets are evident. The activation threshold for the aerosol particles is about 0.16 μm (i.e., the size separating channels 2 and 3 of the PCASP). This threshold value is smaller than for the smooth-air cloud of flight 34, and the difference is consistent with the higher N_d/N_a and $\sigma_{w'}$ for flight 14 than flight 34.

3.3. Physical Observations for All Low Clouds

The relationships among N_d and N_a, $\sigma_{w'}$ and cloud water chemistry are investigated using the data from all 14 flights in marine stratus. The N_a were estimated using observations made just below cloud, during level flight when the aircraft momentarily encountered clear air (e.g., flight 34 at 847-885 s), or just above cloud (e.g., flight 14 at 1363-1423 s). The 1 s N_d and LWC were averaged over the entire in-cloud time (i.e., only 1 s data for which $N_d > 10$ cm^{-3} were used in the average), unless changes in altitude of >100 m were made or if the cloud sampling was split into intervals separated by long times. In the case of either of the latter two conditions, then separate averages were made. For each of flights 14 and 34, for example, one average was determined for the entire in-cloud period. A total of 25 data points resulted from this analysis, and the in-cloud averaging times ranged from 1 to 32 min (about

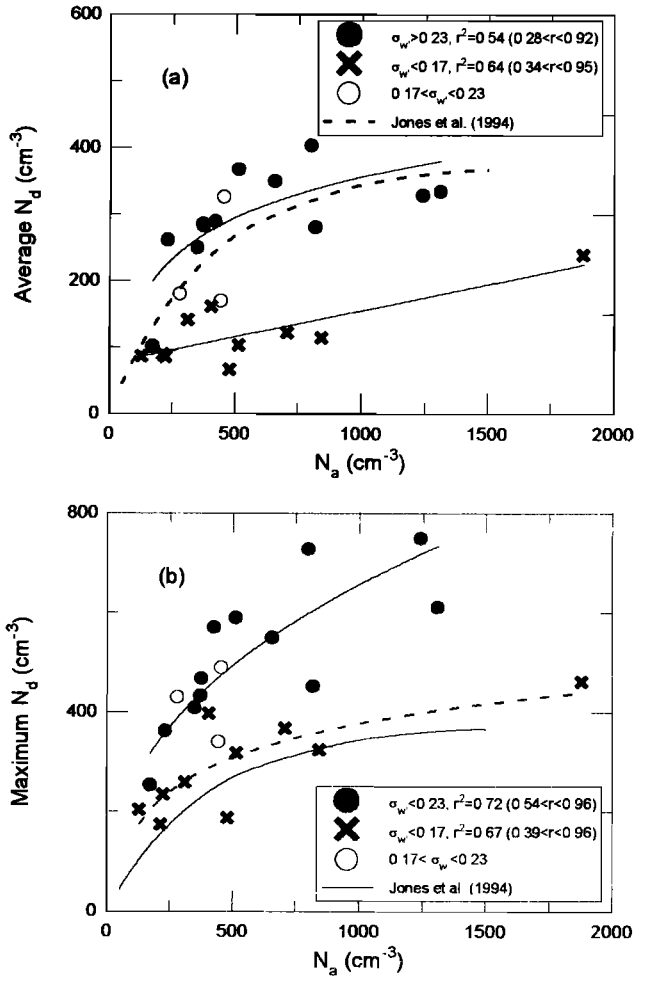

Figure 8. (a) The average N_d and (b) the maximum N_d plotted against the N_a for all flights. The data are separated according to the ranges of $\sigma_{w'}$ indicated in the legend, and curves are fitted to the data for the higher and lower $\sigma_{w'}$. The r^2 values and the 95% confidence limits for r are also given in the legend. The dashed curve is the parameterization used by *Jones et al.* [1994].

3-100 km) with a median time of 10 min. The maximum N_d and the in-cloud $\sigma_{w'}$ were also determined for each average.

Figures 8a and 8b show the average N_d and maximum N_d, respectively, plotted as a function of the N_a. The data are grouped for $\sigma_{w'} < 0.17$ m s^{-1}, $\sigma_{w'} > 0.23$ m s^{-1}, and $0.17 < \sigma_{w'} < 0.23$ m s^{-1}, since a $\sigma_{w'}$ of 0.2 m s^{-1} approximates the distinction between smooth and lightly turbulent air. The $0.17 < \sigma_{w'} < 0.23$ group was chosen as a transition region to reduce overlap due to uncertainty in $\sigma_{w'}$. The complete range of $\sigma_{w'}$ values is about 0.08-0.8 m s^{-1}, but only two values are >0.32 m s^{-1}. Coincidentally, the median $\sigma_{w'}$ (0.19 m s^{-1}) falls close to the smooth-lightly turbulent air distinction. The separation of the N_d versus N_a data by $\sigma_{w'}$ yields relatively distinct groups of data for the lower $\sigma_{w'}$ and higher $\sigma_{w'}$ and significantly increases the ability of the N_a to explain the variance in the N_d. Functions were fitted to the lower and higher $\sigma_{w'}$ groups from a choice of linear or logarithmic forms. Logarithmic functions were selected in addition to a linear function since the frequency distributions of atmospheric data often have logarithmic tendencies, the relationship between N_d

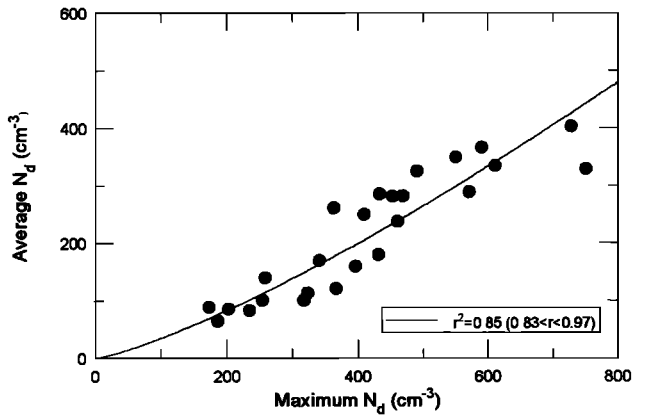

Figure 9. The average N_d versus the maximum N_d for all flights. The r^2 value for the fitted curve and the 95% confidence limits for r are given in the legend.

and N_a has been previously shown to be non-linear [*Leaitch et al.*, 1986], and the theoretical relationship between these two quantities is relatively complex. The fit with the highest coefficient of determination (r^2) is shown for each set of data. The best fits for the groups of data in Figure 8 have a logarithmic form, with the exception of the lower-$\sigma_{w'}$ average-N_d data for which the best fit is linear. The 95% confidence limits for the r are given in parentheses.

There is a strong relationship between the average and the maximum N_d, as shown in Figure 9. This gives rise to the similarity between the N_d-N_a relationships for the average N_d and the maximum N_d. Figure 10 shows the average N_d plotted against the $\sigma_{w'}$. Here, the data have been subdivided based on the median N_a of 445 cm^{-3}. The data are grouped for N_a <400 cm^{-3}, N_a >500 cm^{-3}, and 400<N_a<500 cm^{-3}. This grouping separates the data but does not have so clear an effect

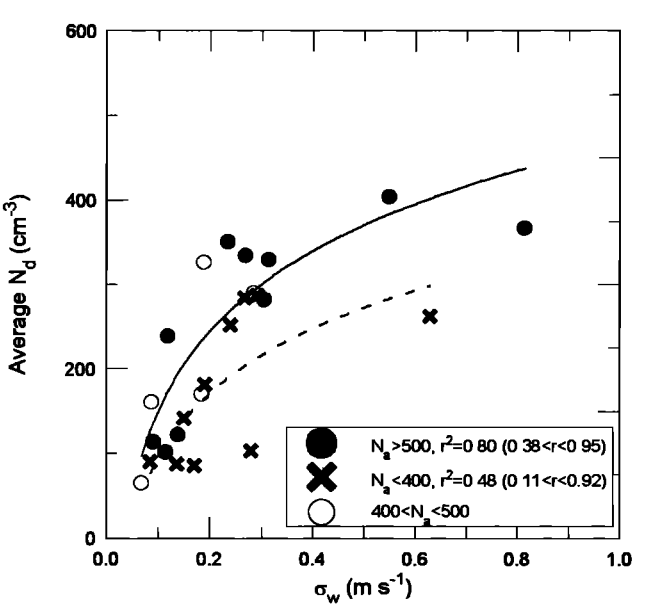

Figure 10. The average N_d versus the $\sigma_{w'}$ for all flights. The data are separated according to the ranges of N_a indicated in the legend, and curves are fitted to the data for the higher and lower N_a. The r^2 values and the 95% confidence limits for r are also given in the legend.

Table 2. Estimated Activation Diameters (Act. Dia.), $\sigma_{w'}$ and N_a for in-Cloud Averages

Cloud ID	Act. Dia. (μm)	$\sigma_{w'}$ (m s^{-1})	N_a (cm^{-3})
8a	0.21	0.14	129
8b	0.14	0.28	170
14	0.16	0.19	454
16	0.18	0.09	413
21	0.21	0.31	1241
34a	0.16	0.32	708
34b	0.21	0.12	708
36	0.18	0.28	368
38a	0.21	0.09	844
38b	0.18	0.31	818
38c	0.16	0.81	512
39a	0.31	0.07	480
39b	0.16	0.55	800
43ab	0.21	0.12	525
43cde	0.16	0.09	212
44a	0.18	0.29	371
44b	0.21	0.15	311
44c	0.18	0.24	403
45a	0.13	0.63	230
45b			
45c	0.21	0.18	445
46a			
46b	0.14	0.27	404
47a	0.18	0.23	655
47b	0.21	0.27	1309
48	0.26	0.12	1879
Median	0.18		

as grouping by $\sigma_{w'}$ had on the N_d-N_a data (Figure 8). In the case of the high N_a the r^2 for the fit is increased relative to that for the complete data set (0.57); however, for the lower N_a, the r^2 is slightly lower. The reduced separation between the lower and the higher N_a, relative to the N_d-N_a plots, suggests that the $\sigma_{w'}$ was more important than the N_a as a controlling factor for the N_d.

3.4. Cloud Activation Sizes of Particles

The minimum sizes of particles activated in these clouds (activation diameter) were estimated through comparisons of the average in-cloud and out-of-cloud PCASP spectra for all the cases presented here. The approach taken is the same as that used for flights 14 and 34 (Figures 5 and 7), except that the in-cloud averages described in section 3.3 were used for the in-cloud spectra. Two averaging periods were used for flight 34 to include the effect of the wave. The results are given in Table 2, together with the corresponding $\sigma_{w'}$ and N_a. The uncertainties in the estimates of the activation diameter are the accuracy of the particle sizing (estimated as the size width of the PCASP bin) and the ability to determine the departure between the out-of-cloud and the interstitial spectra (also one PCASP size bin). No estimates are presented for 45b and 46a because the distinctions between the out-of-cloud spectra were not sufficiently clear; the interstitial spectra did not drop to near zero above the activation diameter, indicating that a few particles larger than this size remained unactivated. The activation diameters range from 0.13 μm to 0.31 μm, with a median of 0.18 μm. Figure 11 shows the activation diameters plotted against N_a and $\sigma_{w'}$. In this figure, higher activation

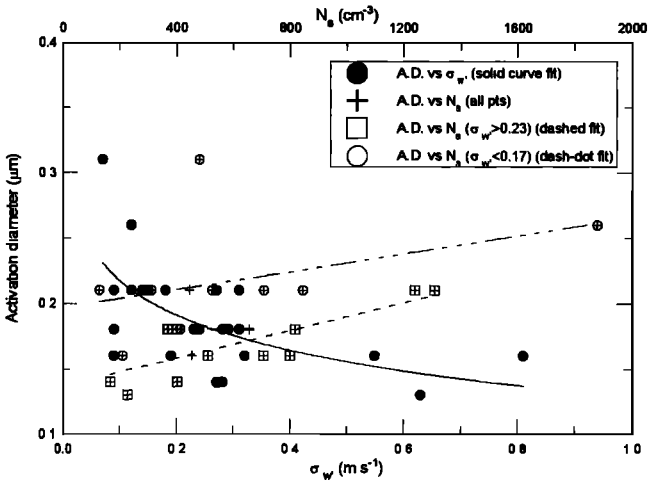

Figure 11. The estimated minimum diameter of particles activated in these stratus (activation diameter) versus the N_a and the $\sigma_{w'}$ based on the data from Table 2. In addition to the complete data set, two groups of the N_a data are identified for smaller variations in $\sigma_{w'}$. The curve fits are used to indicate the tendencies of the data points.

diameters are associated with lower $\sigma_{w'}$. The activation diameter versus N_a data are identified for $\sigma_{w'} < 0.17$ m s^{-1} and $\sigma_{w'} > 0.23$ m s^{-1}. For the higher $\sigma_{w'}$ data the activation size tends to increase with higher N_a. For the lower $\sigma_{w'}$ data there is a very weak tendency for the activation size to increase with increasing N_a. The smaller activation diameters for higher(lower) $\sigma_{w'}(N_a)$ are consistent with the higher N_d/N_a for higher(lower) $\sigma_{w'}(N_a)$ demonstrated by Figure 8.

3.5. Chemical Observations

Twenty eight samples of cloud water were collected from the marine stratus and analyzed for major inorganic and organic ion concentrations. There are incomplete microphysical data for the time of collection of one sample, and the concentrations in seven pairs of samples, collected simultaneously, have been averaged, making a total of 20 data points. The physical data have been averaged over the in-cloud collection time of each sample, which ranges from about 2 to 23 min. The ion concentrations and corresponding physical data averages for the 20 points are given in Table 3. The aqueous concentrations have been converted to equivalent air-volume units (nanoequivalents per cubic meter), using the LWC. Percentiles (25th, 50th and 75th) for the cloud water data are also given. The Chebogue Point observations are pertinent here, since this site was sampling aerosol in the marine boundary layer, and often downwind of the low clouds. The Chebogue Point percentiles at the bottom of Table 3 are for the aerosol measurements identified by *Liu et al.* [this issue] as having been processed through these low marine stratus (50% of the full data set reported by Liu et al.).

Sulfate and nitrate were the principal anions in the cloud water. The median cloud water $SO_4^=$ concentration ($cwSO_4^=$) is somewhat lower than the median Chebogue Point aerosol $SO_4^=$ concentration. This is consistent with the activation of

Table 3. Ion Concentrations and Corresponding Physical Parameter Averages for Cloud Water Samples

Flight	Sample ID	ACE^-	FOR^-	MSA^-	Cl^-	NO_3^-	$SO_4^=$	$C_2O_4^=$	Na^+	NH_4^+	Mg^{++}	Ca^{++}	H^+	Pres. (mbar)	Alt. (m)	Temp. (°C)	N_d (cm^{-3})	LWC (g m^{-3})	$\sigma_{w'}$ (m s^{-1})	N_a (cm^{-3})
8	18			<0.2	12	2.7	9.9	0.9	8.9	<0.7	<1.4	<1.4	15	953	525	15.5	96	0.39	0.28	150
8	11	3.3	2.2	0.2	7.0	2.7	5.7	0.3	5.0	0.8	0.6	0.4		953	523	15.5	111	0.20	0.29	150
14	6&7			0.4	9.6	12	60	1.3	29	9.4	1.3	1.7		999	161	14.6	304	0.25	0.19	454
14	9,10&19			0.4	5.6	8.9	55	3.8	5.9	16	<1.5	<1.5	45	999	163	14.7	335	0.16	0.18	454
16	26	<0.9	<3	0.2	36	15	28	0.2	36	1.2	4.2	2.1		1005	108	16.1	151	0.11	0.09	405
21	55			0.1	3.2	20	113	1.3	2.0	11	<0.6	<0.6	130	956	407	16.4	352	0.11	0.31	1240
34	63			0.6	9.1	59	69	0.9	2.9	13	<0.7	<0.7	109	989	202	18.7	145	0.17	0.18	708
34	38			0.4	15	76	87	<0.2	8.1	15	1.4	2.4		993	170	18.6	118	0.24	0.14	708
36	76			0.2	14	21	46	0.2	11	11	2.5	1.5	60	948	605	14.2	291	0.15	0.24	470
38	53&54			0.2	10	29	56	1.7	9.5	16	1.5	2.7	56	974	345	21.1	119	0.26	0.09	818
39	95	3.5	9.3	0.3	35	42	56	<0.2	35	19	4.4	5.1	45	963	412	21.5	369	0.41	0.60	400
39	97			0.2	10	9.7	21	0.7	7.0	6.8	1.0	1.5	19	976	300	22.4	74	0.24	0.07	400
43	17&102			<0.1	<0.1	1.9	4.1	0.2	<0.4	0.5	<0.4	<0.4	8.3	1000	151	13.2	68	0.23	0.13	213
43	103			<0.08	0.6	4.9	21	<0.2	<0.5	3.2	<0.5	<0.5	22	987	259	14.5	89	0.19	0.11	515
44	89			0.2	0.5	0.8	2.9	0.06	0.2	0.7	<0.2	<0.2	4.2	985	275	16.5	159	0.18	0.23	310
44	93			0.06	2.6	4.8	17	<0.2	0.7	4.9	<0.3	<0.3	18	981	303	16.3	234	0.20	0.23	350
45	137&141			0.05	1.4	19	41	0.5	<0.4	5.2	<0.4	<0.4		959	489	13.6	180	0.13	0.19	278
45	126&140			<0.2	<0.4	33	47	0.7	2.9	6.2	2.5	7.3		977	343	14.1	114	0.16	0.16	445
46	130			0.2	1.0	14	36	0.9	4.7	7.1	<0.2	0.4	40	929	756	12.9	291	0.25	0.28	374
47	119	4.3	8.4	0.3	3.4	39	91	0.05	<0.2	23	<0.2	0.5	107	920	844	14.0	358	0.20	0.26	1048
Median		3.4	5.3	0.2	6.3	15	44	0.4	4.9	7.0	0.8	<1.1	42.3	977	323	15.5	155	0.20	0.19	425
25th percentile				<0.1	1.2	4.9	19	<0.2	0.5	2.2	<0.4	<0.5	18	955	194	14.2	110	0.16	0.14	340
75th percentile				0.3	10	31	56	0.9	9.2	12	1.5	1.9	59	990	498	17.0	295	0.24	0.27	565
C.P. Median				0.7	10	13	69	3.6	32	38	4	<5								460
25th percentile				0.4	<6	<1	51	2.1	5.0	28	<1	<5								340
75th percentile				1.7	42	17	90	4.8	55	59	11	<5								850

All chemical units are nEq m^{-3}; less than indicates below value; blank indicates no analysis; C.P. - Chebogue Point (the C.P. percentiles are from the data of *Liu et al.* [this issue] for aerosol believed to have been processed by low stratus); Pres., pressure; Alt., altitude; Temp., temperature.

only a fraction the sulfate-bearing fine particles; the results of *Liu et al.* [this issue] suggest that sulfate was present in particles both smaller and larger than the activation sizes in Table 2. Much of the Chebogue Point aerosol NO_3^- was associated with Na^+, from the reaction of HNO_3 with N_aCl either in the atmosphere or on the collection filters [*Liu et al.*, this issue]. The relatively close agreement between the $cwNO_3^-$ and Chebogue Point NO_3^- medians can then be explained as due to the efficient scavenging of nitrate by these clouds if its presence before cloud was as HNO_3 and/or an aerosol salt associated with larger particles (e.g., $NaNO_3$).

The medians of Na^+, Cl^-, methanesulfonate (MSA^-), NH_4^+, and oxalate ($C_2O_4^=$) are all lower in the cloud water compared with the Chebogue Point aerosol. Because of the relative calm sea conditions during the study, it is likely that the concentrations of sea-salt particles were higher nearer the surface than aloft. Also, because of the coastal location, local sea-salt generation may have occasionally influenced the Chebogue Point sampling. Thus the higher cloud water sampling altitudes relative to Chebogue Point can explain the lower $cwNa^+$, $cwCl^-$ (in which case the NO_3^- scavenged by the cloud was more HNO_3 than $NaNO_3$), and perhaps the $cwMSA^-$. The lower $cwNH_4^+$ compared with Chebogue Point and the high $cwH^+/cwNH_4^+$ indicates that the low clouds were more acidic than would have resulted from the dissolution of the aerosol sampled at Chebogue Point. The Chebogue Point aerosol may have reacted with NH_3 from local sources before or during sampling at the site. Oxalate sampled at Chebogue Point was primarily associated with particles smaller than about 0.2 μm [Liu et al.]. Thus the lower $cwC_2O_4^=$ is consistent with the inactivation of the smaller particles (<0.2 μm) in these clouds (Table 2).

Figure 12 shows the relationships of the $cwSO_4^=$ and $cwNO_3^-$ with the N_a. There is a good relationship between the $cwSO_4^=$ and the N_a, consistent with this ion making a large contribution to the accumulation-mode aerosol and being strongly associated with particles activated in cloud. The relationship for $cwNO_3^-$ is weaker due to lower concentrations than $cwSO_4^=$, and/or because much of the $cwNO_3^-$ can have its source in the gas phase (e.g., HNO_3), [*Daum et al.*, this issue].

The N_d has been shown to be related to $cwSO_4^=$ for continental clouds [*Leaitch et al.*, 1992], and *Kulmala et al.* [1993] have shown that HNO_3 can influence the N_d. Plots of the N_d versus the $cwSO_4^=$ and $cwNO_3^-$ are shown in Figures 13a and 13b, respectively. The r^2 for the regressions to all of the data are 0.30 and 0.12 for $cwSO_4^=$ and $cwNO_3^-$, respectively (the $cwSO_4^=$ result is significant at the 95% confidence, but the $cwNO_3^-$ is not). Separation of the data using the same criteria as for the N_d versus N_a yields two distinct groups, one with higher N_d corresponding to the higher $\sigma_{w'}$ and the other with lower N_d corresponding to the lower $\sigma_{w'}$. This separation substantially increases the ability to explain the variance in the N_d, particularly for the $cwNO_3^-$.

4. Discussion

The regression curves in Figures 8 and 13 show that the N_d increase with increasing N_a and $cwSO_4^=$, but the rate of increase of N_d decreases with increasing N_a and $cwSO_4^=$. This result is consistent with that predicted by *Jensen and Charlson* [1984] and with the observations of *Leaitch et al.* [1986], *Hallberg et al.* [1994], and *Gillani et al.* [1995]. The physical and chemical nature of the CCN and competition for water vapor contribute to the nonlinearity of these relationships.

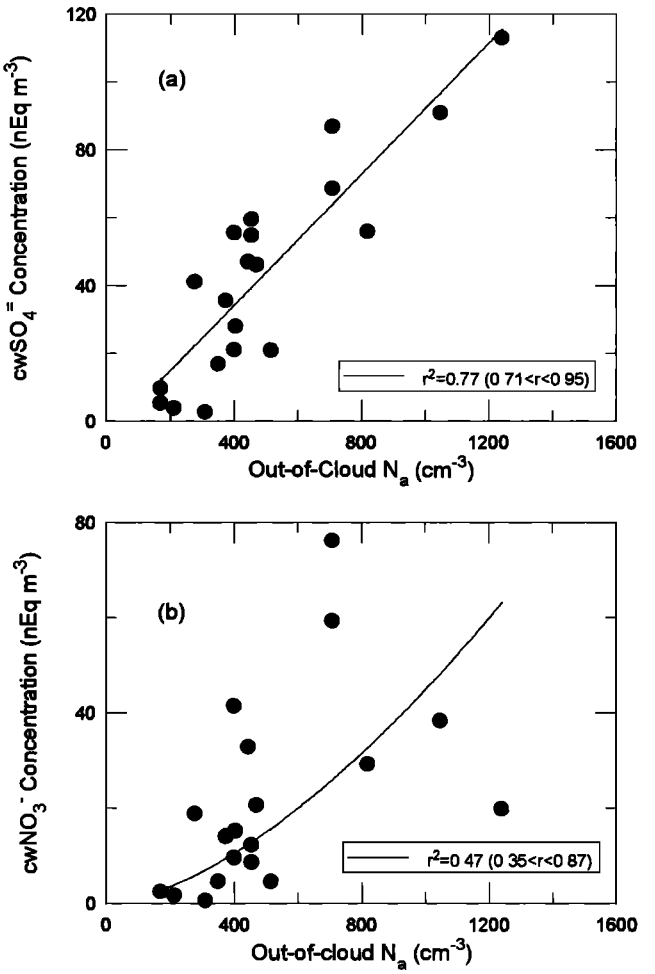

Figure 12. (a) The cloud water $SO_4^=$ concentrations and (b) the cloud water NO_3^- concentrations plotted against the N_a. The r^2 values for the fitted curves and the 95% confidence limits for r are given in the legend.

The estimated activation diameters for the aerosol particles ranged from 0.13 μm to 0.31 μm. Based on the CCN observations at Chebogue Point [*Liu et al.*, this issue], this corresponds to average supersaturations in these clouds of $\leq 0.1\%$. This compares with the result of *Hudson* [1984] who found from CCN measurements in fogs that particles active at $>0.12\%$ supersaturation were not activated. The activation diameters are also consistent with the explanation for the differences in the aerosol size distributions noted at the Chebogue Point depending on whether low stratus was present or not [Liu et al.]. Liu et al. found that more particle volume was associated with particles larger than about 0.2 μm and that sulfate had a higher statistical association with larger particle sizes when low stratus was present. This was explained by Liu et al. as being due to the addition of small and reasonable quantities of sulfate to particles larger than about 0.2 μm via S(IV) oxidation in these clouds. These results concur well with those of *Hoppel et al.* [1986, 1990, 1994], who have discussed the potential impact of S(IV) oxidation on the aerosol particle size distribution in

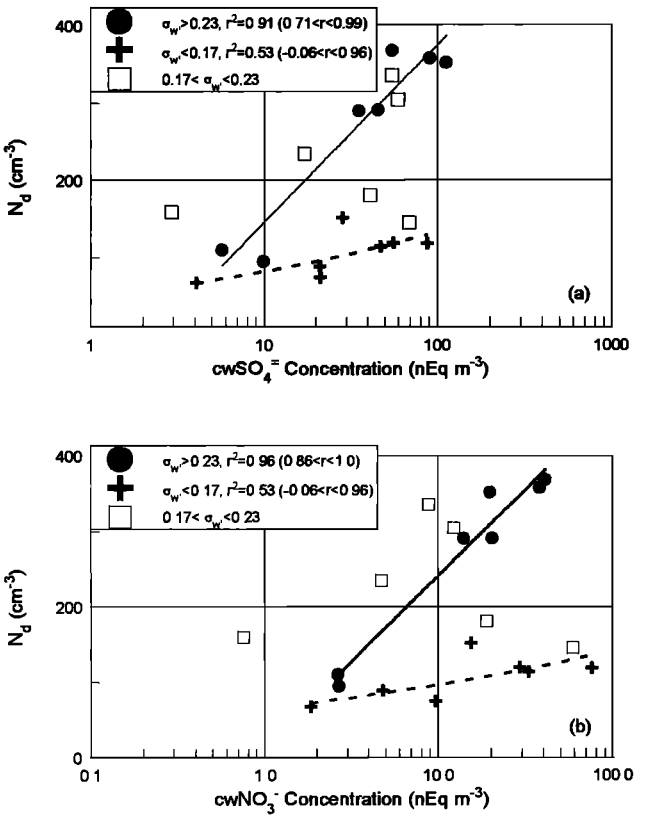

Figure 13. (a) The average N_d plotted against the cloud water $SO_4^=$ concentrations and (b) the cloud water NO_3^- concentrations. The data are separated according to the ranges of $\sigma_{w'}$ indicated in the legend, and curves are fitted to the data for the higher and lower $\sigma_{w'}$. The r^2 values and the 95% confidence limits for r are also given in the legend.

marine stratus over both the Atlantic and the Pacific Oceans. Aerosol observations made outside of Pacific marine stratus reported by *Anderson et al.* [1994] indicate a minimum at 0.1 μm or below, which suggests a lower activation diameter in their clouds. This might be explained by a significant orographic influence that was noted for their measurement site.

The data in Figures 8 and 10 suggest that the influence of turbulence on the N_d is stronger than that of the N_a. Also, the change from smooth air to light turbulence appears to increase the relative impact of the aerosol on the N_d. The fits in Figure 8a show that changes in the average N_d for the same change in the N_a are larger for the higher $\sigma_{w'}$ compared with the lower $\sigma_{w'}$ by factors ranging from 1.3 to 3.1. A similar result is indicated for the effect of turbulence on the relationships between the N_d and the concentration of major ions in cloud water (Figure 13). These results are consistent in a general sense with the analytical result of *Twomey* [1959] which indicates that for situations with lower supersaturations, as here, the N_d are more strongly controlled by the updraft velocity than by the N_a. The enhancement in the N_d for higher $\sigma_{w'}$ results from the fact that there are relatively higher number concentrations of particles present at smaller particle sizes. Increasing turbulent mixing would lead to a more rapid cooling rate during ascent and a higher supersaturation. This would be compensated for in part by the corresponding downdraft. However, as *Korolev* [1995] has demonstrated, the effect of the solute in the droplets means that many of the droplets only partially evaporate in the downdraft.

Jones et al. [1994] used a general circulation model to estimate the global indirect cooling effect due only to changes in cloud reflectance from increased N_d. They used the data of *Martin et al.* [1994] to obtain a parameterization of the change in the N_d with changes in aerosol particle concentration. The Jones et al. parameterization is shown in Figure 8. There is reasonable agreement between the Jones et al. curve and the average N_d versus N_a relationship for the higher $\sigma_{w'}$, but the agreement with the lower-$\sigma_{w'}$ average N_d versus N_a is poor.

A comparison of the N_d-$cwSO_4^=$ data with the stratiform cloud data from *Leaitch et al.* [1992] is presented in Figure 14. The higher-$\sigma_{w'}$ data group compares reasonably well with the regression from Leaitch et al., while the lower-$\sigma_{w'}$ data are mostly at the lower N_d portion of the Leaitch et al. data. This result is consistent with higher turbulence over the continent. One difficulty with this relationship in general is that S(IV) oxidation may increase the $cwSO_4^=$ without influencing the N_d. In the case of the NARE observations, the Chebogue Point data [*Liu et al.*, this issue] suggest that for periods with stratus offshore the average contribution from S(IV) oxidation was about 30-50% of the non-sea-salt $SO_4^=$. Thus the $cwSO_4^=$ concentrations in Figure 14 may overestimate the sulfate concentrations in the precloud aerosol. On the other hand, the fact that the activation of particles stops at a size of about 0.2 μm, on average, means that smaller particles of sulfate were not activated. From the data of Liu et al. it is estimated that from 10 to 40% of the accumulation-mode mass may have remained unactivated. For this reason, the $cwSO_4^=$ concentrations in Figure 14 may underestimate the precloud particulate sulfate.

There was a variety of N_a and major ion concentrations associated with these low stratus. However, the N_a in and below these clouds and the major ion concentrations in these clouds were often much lower than observed in the aerosol above the cloud [*Kleinman et al.*, this issue (a); *Banic et al.*,

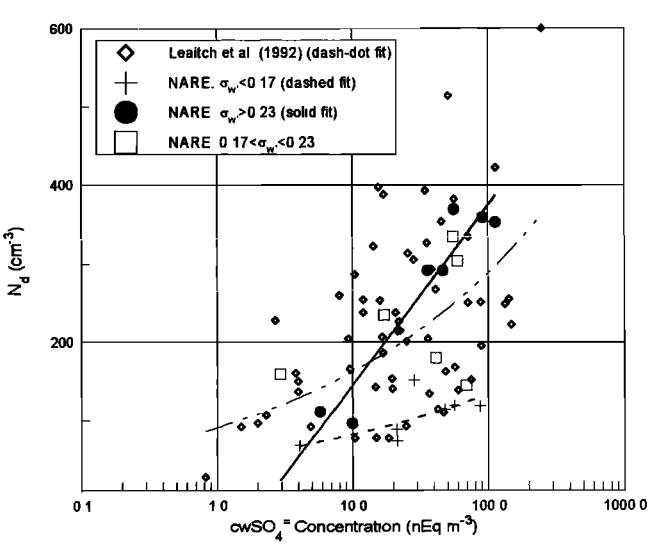

Figure 14. The average N_d versus cloud water $SO_4^=$ concentrations for the data from Leaitch et al. [1992] and the North Atlantic Regional Experiment (NARE) data. The NARE data are separated according to the ranges of $\sigma_{w'}$, as in Figure 13.

this issue; *Li et al.*, this issue]. The air back trajectories (Figure 1) indicate that there is no connection of the 1000 mbar air in the region of Yarmouth with the main anthropogenic source regions of eastern North America during these cloud events. Even when the stratus was sampled at higher altitudes (e.g., flights 45-47), the main anthropogenic plume from the continent overrode this cloud, as demonstrated by the profile data of flight 45 (Figure 2). This may change as the air moves eastward and over the Gulf Stream.

5. Summary and Conclusions

Physical and chemical observations were made in and around marine stratus on 14 flights during the 1993 NARE intensive. The observations were made over the Gulf of Maine within 50 km of Nova Scotia and over the Bay of Fundy. The clouds formed in warmer air over cooler water and, at times, had a fog layer underneath. Although the clouds sampled were never directly impacted by the main anthropogenic plume from North America, some of the precloud aerosol was transported from the continent, and a wide range of particle loadings was associated with the clouds. The median sampling altitude, liquid water content, and temperature were 320 m, 0.20 g m^{-3}, and 16°C, respectively. The observations were used to address questions pertaining to the control of cloud droplet number concentrations (N_d) by aerosol particles, cloud water chemistry, and the presence of light turbulence.

The minimum diameters of the particles activated in these clouds were estimated through comparison of the cloud interstitial particle spectra with the out-of-cloud particle spectra. The activation thresholds range from 0.13 μm to 0.31 μm with a median value of 0.18 μm, corresponding to supersaturations of $<0.1\%$. The higher activation sizes were associated with either or both of lower σ_w. and higher N_a.

There was a weak positive dependence of the N_d on the outside-of-cloud aerosol particle number concentration (N_a). The dependence strengthened when the data were separated between smooth and lightly turbulent air. The relationships were non-linear, for the range of observed N_a, with the rate of increase of N_d decreasing with increasing N_a. The data for cases with light turbulence were in close agreement with the function used by *Jones et al.* [1994] to model the global indirect cooling by aerosols. The data for smooth air did not agree with that used by Jones et al.

Sulfate and nitrate were the dominant anions measured in 28 cloud water samples collected in the marine stratus. The cloud water $SO_4^=$ concentrations ($cwSO_4^=$) were positively related to the N_a and, to a lesser degree, so were the cloud water NO_3^- concentrations ($cwNO_3^-$). For all the data, $cwSO_4^=$ and $cwNO_3^-$ explained about 30% and 12% of the variance in the N_d, respectively. For the data separated between smooth air and lightly turbulent air, the ability of $cwSO_4^=$ and $cwNO_3^-$ to explain the variance in the N_d increased significantly. The N_d-$cwSO_4^=$ relationship for light turbulence was close to the relationship obtained by Leaitch et al. [1992] for continental stratiform cloud, and the smooth-air data coincided with the lower N_d part of the Leaitch et al. data envelope. The relationships of the N_d with the major ions are consistent with those for the N_d-N_a.

Turbulence in these clouds appears to be a significant factor for the determination of the N_d. In addition, changes in the N_d were more sensitive to changes in the N_a or $cwSO_4^=$ for the lightly turbulent air than for the smooth air. This suggests that cloud turbulence is also important for its potential influence on the effect of aerosol particles on the N_d. More knowledge of the physical factors controlling the N_d in stratiform clouds, such as turbulence, is needed to improve not only our ability to represent N_d, but to increase our understanding of the impact of the aerosol particles on the N_d and climate.

Acknowledgments. The authors are very grateful to J. Aitken, M. Morgan, and C.Taylor of the NRC-Canada, and S. Bacic, R. Poersch, D. Tallon, M. Wasey, J. Abraham, D. Wartman, and D. Waugh of the AES for their assistance in the field. We would also like to thank the manager and staff of the Yarmouth Airport for their support.

References

Anderson, T.L., D.S. Covert, and R.J. Charlson, Cloud droplet number studies with a counterflow virtual impactor, *J. Geophys. Res.*, *99*, 8249-8256, 1994.

Angevine, W.M., and J.I. MacPherson, Comparison of wind profiler and aircraft wind measurements at Chebogue Point, Nova Scotia, *J. Atmos. Oceanic Technol.*, *12*, 421-426, 1995.

Angevine, W.M., M. Trainer, S.A. McKeen, and C. Berkowitz, Mesoscale meterology of the New England coast, Gulf of Maine, and Nova Scotia: Overview, *J. Geophys. Res.*, this issue.

Arends, B.G. et al., Microphysics of clouds at Kleiner Feldberg, *J. Atmos. Chem.*, *19*, 59-85, 1994.

Banic, C.M., W.R. Leaitch, G.A. Isaac, M.D. Couture, L.I. Kleinman, S.R. Springston and J.I. MacPherson, Transport of ozone and sulfur to the North Atlantic atmosphere during NARE, *J. Geophys. Res.*, this issue.

Baumgardner, D., J.W. Strapp, and J.E. Dye, Evaluation of the forward scattering spectrometer probe, II, Corrections for coincidence and dead time errors, *J. Atmos. Oceanic Technol.*, *2*, 626-632, 1985.

Brook, J.R., P.J. Sampson and S. Sillman, The relationship between upwind SO2 emissions and SO4= concentrations in precipitation at six sites in the eastern U.S.A., *Atmos. Environ.*, *27A*, 1765-1779, 1993.

Charlson, R.J., S.E. Schwartz, J.M. Hales, R.D. Cess, J.A. Coakley Jr., J.E. Hansen, and D.J. Hofmann, Climate forcing by anthropogenic aerosols, *Science*, *255*, 423-430, 1992.

Chylek, P. et al., Black carbon: atmospheric concentrations and cloud water content measurements over southern Nova Scotia, *J. Geophys. Res.*, this issue.

Cober, S.G., G.A. Isaac, and J.W. Strapp, Aircraft icing measurements in east coast winter storms, *J. Appl. Meteorol.*, *34*, 88-100, 1995.

Daum, P.H., L.I. Kleinman, L. Newman, W.Luke, J. Weinstein-Lloyd, C.M. Berkowitz and K. Busness, Chemical and physical properties of plumes of anthropogenic pollutants transported over the North Atlantic during NARE, *J. Geophys. Res.*, this issue.

Gillani, N., W.R. Leaitch, J.W. Strapp and G.A. Isaac, Field observations in continental stratiform clouds: partitioning of cloud droplets between droplets and unactivated interstitial aerosols. *J. Geophys. Res., 100,* 18687-18706, 1995.

Gultepe, I., G.A. Isaac, W.R. Leaitch, and C.M. Banic, Parameterizations of marine stratus microphysics based on in-situ observations: implications for GCMs. *J. Clim., 9,* 345-357, 1996.

Hallberg, A. et al., Phase partitioning of aerosol particles in clouds at Kleiner Feldberg, *J. Atmos. Chem., 19,* 107-127, 1994.

Hoppel, W.A., G.M. Frick, and R.E. Larson, Effect of non-precipitating clouds on the aerosol size distribution, *Geophys. Res. Lett., 13,* 125-128, 1986.

Hoppel, W.A., J.W. Fitzgerald, G.M. Frick, R.E. Larson, and E.J. Mack, Aerosol size distributions and optical properties found in the marine boundary layer over the Atlantic Ocean, *J. Geophys. Res., 95,* 3659-3686, 1990.

Hoppel, W.A., G.M. Frick, J.W. Fitzgerald, and R.E. Larson, Marine boundary layer measurements of new particle formation and the effects of nonprecipitating clouds on the aerosol size distribution, *J. Geophys. Res., 99,* 14,443-14,459, 1994.

Hudson, J.G., Cloud condensation nuclei measurements within clouds, *J. Clim. Appl. Meteorol., 23,* 42-51, 1984.

Intergovernmental Panel on Climate Change (IPCC), Radiative forcing of climate change and an evaluation of the IPCC IS92 emission scenarios, in climate change 1994, *Cambridge Univ. Press,* New York, 1995.

Jensen, J.B., and R.J. Charlson, On the efficiency of nucleation scavenging, *Tellus, 36B,* 367-375, 1984.

Jones, A., D.L. Roberts, and A. Slingo, A climate model study of indirect radiative forcing by anthropogenic aerosols, *Nature, 370,* 450-453, 1994.

Kim, Y.J., Response of the active scattering aerosol spectrometer probe (ASASP-100X) to particles of different composition, *Aerosol Sci. Technol., 22,* 33-42, 1995.

Kleinman, L.I., P.H. Daum, Y.-N. Lee, S.R. Springston, L. Newman, W.R. Leaitch, C.M. Banic, G.A. Isaac, and J.I. MacPherson, Measurement of O3 and related compounds over southern Nova Scotia, 1, Vertical distributions, *J. Geophys. Res.*, this issue (a).

Kleinman, L.I., P.H. Daum, S.R. Springston, W.R. Leaitch, C.M. Banic, G.A. Isaac, B.T. Jobson, and H. Niki, Measurement of O3 and related compounds over southern Nova Scotia, 2, Photochemical age and vertical transport, *J. Geophys. Res.*, this issue (b).

Korolev, A., The influence of supersaturation fluctuations on droplet size spectra formation, *J. Atmos. Sci., 52,* 3620-3634, 1995.

Kulmula, M., A. Laaksonen, P. Korhonen, T. Vesala, and T. Ahonen, The effect of atmospheric nitric acid vapor on cloud condensation nucleus activation, *J. Geophys. Res., 98,* 22,949-22,958, 1993.

Leaitch, W.R., J.W. Strapp, G.A. Isaac, and J.G. Hudson, Cloud droplet nucleation and cloud scavenging of aerosol sulphate in polluted atmospheres, *Tellus, 38B,* 328-344, 1986.

Leaitch, W.R., G.A. Isaac, J.W. Strapp, C.M. Banic, and H.A. Wiebe, The relationship between cloud droplet number concentrations and anthropogenic pollution: observations and climatic implications, *J. Geophys. Res., 97,* 2463-2474, 1992.

Li, S.-M., C.M. Banic, W.R. Leaitch, P.S.K. Liu, G.A. Isaac, X.-L. Zhou, and Y.-N. Lee, Water-soluble fractions of aerosol and the relations to number size distributions based on aircraft measurements from the North Atlantic Regional Experiment, *J. Geophys. Res.*, this issue.

Liu, P.S.K., W.R Leaitch, J.W. Strapp and M.A. Wasey, Response of Particle Measuring Systems airborne ASASP and PCASP to NaCl and latex particles, *Aerosol Sci. Technol., 16,* 83-95, 1992.

Liu, P.S.K., W.R. Leaitch, C.M. Banic, S.-M. Li, D. Ngo, and W.J. Megaw, Aerosol observations at Chebogue Point during the NARE 1993: Relationships among CCN, size distribution, and chemistry, *J. Geophys. Res.*, this issue.

MacPherson, J.I., Wind and flux calculations on the NAE Twin Otter, *LTR-FR-109, Nat. Res. Council of Can.*, Ottawa, 1990.

Martin, G.M., D.W. Johnson, and A. Spice, The measurement and parameterization of effective radius of droplets in warm stratocumulus clouds, *J. Atmos. Sci., 51,* 1823-1842, 1994.

Novakov, T., C. Rivera-Carpio, J. Penner, and C.F. Rogers, The effect of anthropogenic sulfate aerosols on marine cloud droplet concentrations, *Tellus, 46B, 132-141,* 1994.

Olson, M.P., K.K. Oikawa, and A.W. MacAfee, A trajectory model applied to the long-range transport of air pollutants, *LRTAP 78-4, Atmos. Environ. Serv.*, Downsview, Ontario, Canada, 1978.

Penner, J.E., R.J. Charlson, J.M. Hales, N.S. Laulainen, R. Leifer, T. Novakov, J. Ogren, L.F. Radke, S.E. Schwartz, and L. Travis, Quantifying and minimizing the uncertainty of climate forcing by anthropogenic aerosols, *Bull. Am. Meteorol. Soc., 75,* 375-400, 1994.

Raga, G.B., and P.R. Jonas, On the link between cloud-top radiative properties and sub-cloud aerosol concentrations, *Q. J. R. Meteorol. Soc., 119,* 1419-1425, 1993.

Twomey, S., The nuclei of natural cloud formation, II; The supersaturation in natural clouds and the variation of cloud droplet concentration, *Geophys. Pure. Appl., 43,* 243-249, 1959.

C.M. Banic, M.D. Couture, I. Gultepe, G.A. Isaac, W.R. Leaitch, S.-M. Li, P.S.K. Liu, Atmospheric Environment Service, 4905 Dufferin Street, Downsview, Ontario M3H 5T4 Canada. (e-mail: armpcb1@dowsv01.dow.on.doe.ca; couture@armph3.dow.on.doe.ca; ismail@armph3.dow.on.doe.ca; isaacg@am.dow.on.doe.ca; leaitch@armph3.dow.on.doe.ca; sli@dow.on.doe.ca; pliu@dow.on.doe.ca)

P.H. Daum, L. Kleinman, Brookhaven National Laboratory, P.O. Box 5000, Upton, NY 11973-5000. (e-mail: phdaum@bnlux1.bnl.gov; kleinman@bnlcl6.bnl.gov)

J.I. MacPherson, Institute for Aerospace Research, National Research Council of Canada, Montreal Road, Building U-61, Ottawa, Ontario K1A 0R6 Canada. (e-mail: macpherson@iaruplands.lan.nrc.ca)

(Received June 20, 1995; revised February 8, 1996; accepted March 28, 1996.)